

RSC Advances



This is an *Accepted Manuscript*, which has been through the Royal Society of Chemistry peer review process and has been accepted for publication.

Accepted Manuscripts are published online shortly after acceptance, before technical editing, formatting and proof reading. Using this free service, authors can make their results available to the community, in citable form, before we publish the edited article. This *Accepted Manuscript* will be replaced by the edited, formatted and paginated article as soon as this is available.

You can find more information about *Accepted Manuscripts* in the [Information for Authors](#).

Please note that technical editing may introduce minor changes to the text and/or graphics, which may alter content. The journal's standard [Terms & Conditions](#) and the [Ethical guidelines](#) still apply. In no event shall the Royal Society of Chemistry be held responsible for any errors or omissions in this *Accepted Manuscript* or any consequences arising from the use of any information it contains.

Anticancer Metallodrugs of Glutamic Acid Sulphonamides: *In Silico*, DNA Binding, Hemolysis and Anticancer Studies

*Imran Ali¹, Waseem A. Wani¹, Kishwar Saleem¹ and Ming-Fa Hsieh²

¹Department of Chemistry
Jamia Millia Islamia (Central University)
New Delhi - 110025, INDIA

²Department of Biomedical Engineering, Chung Yuan Christian University, 200,
Chung Pei Rd., Chung Li, Taiwan

*Correspondence: drimran_ali@yahoo.com, drimran.chiral@gmail.com

Phone No.: 0091-9211458226, Fax No.: 0091-11-26985507

Abstract:

In response to an increased demand for effective anticancer drugs, a series of disodium sulphonamides of L-glutamic acid (L1-L3) was synthesized. Sulphonamides were complexed with copper(II), nickel(II) and ruthenium(III) ions, separately and respectively. Sulphonamides and their complexes were characterized by various physico-chemical, analytical and spectroscopic techniques. Solution stability studies indicated robust nature of the complexes in PBS at 7.4 pH. DNA binding constants (K_b) revealed good binding (0.7×10^3 - 5.24×10^4 mole⁻¹) capacities of the reported compounds. Complexes bound to DNA more efficiently as compared to their ligands. *In silico* studies supported DNA binding of the reported ligands. A cumulative opinion from the results of *in silico* and DNA binding studies indicated that the polarizing and non-polarizing effects of chloro and methyl groups significantly affected the DNA binding ability of the compounds. The compounds were less toxic towards rabbit RBCs as compared to well-known anticancer drug doxorubicin. All the compounds had good anticancer activities (131-53 % viability) on MCF-7 (wild type) cell lines.

Keywords: Sodium sulphonamides, Solution stability studies, *In Silico* studies, DNA binding, Hemolytic assays and Anticancer profiles.

Introduction

Cancer has been a big threat to human beings from a long time. The numbers of cancer patients are increasing continuously. Many factors contribute to increasing cancer genesis, among which modernization of our society is one of the major contributing factors [1,2]. Despite of several anticancer drugs available in the market, cancer kills millions of people every year, globally. Besides, the available anticancer drugs pose serious side effects, which limit their uses considerably [3-5]. Therefore, the demand for an ideal anticancer drug that can control this disease even at late stages with no or less side effects, still continues.

Glutamine (a glutamic acid derivative) is an essential growth component for proliferating tumor cells. Probably, it is the most abundant free amino acid in human body; essential for the growth of normal and neoplastic cells. Tumors are known to produce great changes in host glutamine metabolism. Overall, glutamine promotes the rapid growth and multiplication of cancer cells. The effects of glutamine on cancer cell growth and multiplication suggested the possibility of a good association between glutamine, glutamic acid and cancer [6]. In addition, the re-introduction of thalidomide (a synthetic glutamic acid derivative) in clinical trials for the treatment of various malignant tumors firmly supported the association of glutamic acid and glutamine with cancer [7,8]. As a result of these findings, it was realized that certain structural variants and analogues of glutamic acid and glutamine might be opposing the effects produced by glutamine in proliferating cancer cells [9]. In this direction, few glutamic acid and glutamine derivatives are synthesized and screened for their antiproliferative effects [10-13]. It was observed that the reported glutamic acid and glutamine derivatives showed fair anticancer activities.

The interesting pharmacology of glutamic acid and its derivatives has been known from a long time ago. In 1948, Farber and coworkers [14] reported the clinical results of the temporary remissions in acute leukemia in children treated with 4-aminopteroyl-glutamic

acid (aminopterin) (Fig. 1); a folic acid antagonist. Later on, Lederle Laboratories (Pearl River, New York) in United States marketed aminopterin from 1953 to 1964 for the treatment of pediatric leukemia. However, Lederle Laboratories simultaneously marketed methotrexate (MTX or amethopterin) (Fig. 1); which later led to the discontinuation of aminopterin due to its toxic side effects. Methotrexate is currently being used either alone or in combination with other agents for the treatment of breast, head and neck, leukemia, lymphoma, lung, osteosarcoma, bladder, and trophoblastic neoplasms. The main side effects associated with the treatment with methotrexate include ulcerative stomatitis, low white blood cell count, nausea, abdominal pain, fatigue, fever, dizziness, acute pneumonitis and in rare cases pulmonary fibrosis [15]. To combat some side effects caused by the therapy with methotrexate; folinic acid (Fig. 1) (another congener of glutamic acid) is administered at the appropriate time following methotrexate medication, which rescues bone marrow and gastrointestinal mucosa cells from methotrexate [16]. Moreover, folinic acid is used in combination chemotherapy with 5-fluorouracil for the treatment of colon cancer. Folinic acid enhances the effect of 5-fluorouracil by the inhibition of thymidylate synthase.

Sulphonamides are an important class of drugs. Some sulphonamides and their derivatives have been observed to exhibit substantial *in vitro* and *in vivo* antitumor activity [17]. The antitumor action of sulphonamides has been attributed to different mechanistic phenomena including carbonic anhydrase inhibition, cell cycle arrest in the G1 phase, microtubule assembly disruption and angiogenesis [17]. Some compounds with basic sulphonamide motifs have been investigated as possible anticancer agents. The results indicated good anticancer activities on different cell lines [18-21].

Appropriate selection of ligands may be used to develop active metallodrugs with various advantages over the organic based drugs. It is due to good affinities of different metals towards DNA. Copper complexes are known for their reputation in cancer

chemotherapy and, therefore, being extensively investigated for the treatment of various cancers [22-25]. Nickel is considered a weak carcinogen. However, reports suggested that nickel interacts with DNA and DNA-binding proteins, and a few reports on the anticancer potentials of nickel complexes are available in the literature [26-29]. Ruthenium anticancer drugs have been extensively explored during the last 20 years and two of them have entered into clinical trials. Ruthenium complexes are, generally, less toxic and capable of overcoming platinum drug resistance in cancer cells [30]. Ruthenium complexes cause selective antimetastasis and have lower systemic toxicity. Moreover, they penetrate reasonably well into tumor cells and, therefore, effectively bind to DNA [31]. In addition, they exhibit ligand exchange kinetics similar to platinum(II) antitumor drugs. Presently, ruthenium complexes are being extensively synthesized and screened for their anticancer activities and quite interesting results are being obtained [32-35]. In the light of these facts, a series of disodium sulphonamides of L-glutamic acid was synthesized. The sulphonamides were complexed with Cu(II), Ni(II) and Ru(III) ions, separately and respectively. The binding of ligands and their complexes with Ct-DNA was studied by UV-Vis. absorption spectrophotometry. Hemolysis assays were carried out on rabbit RBCs and the anticancer profiles were determined on MCF-7 (wild type) cell lines. The results of DNA binding of the ligands were verified by *in silico* studies. The results of these findings are presented herein.

Experimental

Materials and Methods

All the reagents were of A.R. grades used without further purification. L-Glutamic acid was purchased from K.C. Biological, Lenexa, Kansas, USA. Benzenesulphonyl chloride, *p*-chlorobenzenesulphonyl chloride and *p*-toluenebenzenesulphonyl chloride were purchased from S.D. Fine Chemicals, Mumbai. RuCl₃.3H₂O was procured from Avarice Lab. Pvt. Ltd., G.B. Nagar, India. CuCl₂.2H₂O, NiCl₂.6H₂O, DMF, ethanol, methanol and hexane were

supplied by E. Merck, Mumbai, India. Pre-coated aluminium silica gel 60 F₂₅₄ thin layer plates were purchased from E. Merck, Germany. Disodium salt of Ct-DNA and tris-(hydroxymethyl) aminomethane were supplied by Sisco Research Lab., Mumbai, India. Human breast cancer cell lines (MCF-7) were collected from the School of Pharmacy, College of Medicine, National Taiwan University. 3-(4,5-Dimethylthiazol-2-yl)-2,5-diphenyl tetrazolium bromide (MTT) was purchased from Sigma-Aldrich (St. Louis, MO, U.S.A.). Dulbecco's modified eagle's medium (DMEM) and antibiotics/antimycotics were purchased from GIBCO (NY, U.S.A.). The fetal bovine serum (FBS) was obtained from HyClone (Utah, U.S.A.).

The percentages of C, H, N and S were determined by a Vario EL elemental analyzer (EL-III). UV-Vis. spectra were recorded on a Perkin Elmer Lambda 40 UV-Vis spectrometer (CT 06859 USA). FT-IR spectra were recorded on a Perkin Elmer RXIFT system spectrometer (LR 64912C) in the range of 4000-400 cm⁻¹ using KBr discs. ¹H NMR spectra were recorded on Bruker 300 MHz instrument (DPX 300). ESI-mass spectra were recorded on micrOTOF-Q II spectrometer (10262). The reactions were monitored by thin layer chromatography using UV Cabinet for visualization. Molar conductivities were recorded on Decibel conductivity meter (DB-1038). pH meter of Control Dynamics (APX 175 E/C) was used to record pH of solutions. Melting points were recorded on Veego instrument (REC-22038 A2). Double distilled water was prepared by a Millipore Milli-Q (Bedford, MA, U.S.A.) water purification system. Molecular modelling studies were carried out by the use of semi-empirical method PM3 as implemented in the hyperchem 8.0 (Hypercube, Inc., USA). *In Silico* studies were carried out by AutoDock 4.2 (Scripps Research Institute, U.S.A.) on Intel® core™ i3 CPU (3.2 GHz) with Windows XP operating system. Incubator for cell culture (MCO-15AC, Sanyo), centrifuge (CN2060, Hsiangtai Co.) and microplate photometer

(Multiskan FC, Thermo Scientific) were used for carrying out the hemolysis and anticancer assays of the developed compounds.

Synthesis of Ligands (L1-L3)

Synthesis of Ligand1 (L1)

0.6 g (15.0 mM) of solid sodium hydroxide was added to a solution of L-glutamic acid (0.735 g, 5 mM) in 50 mL methanol. The resulting mixture was refluxed with stirring till all the glutamic acid dissolved completely. To this neutralized solution, a solution of 0.96 mL (7.5 mM) of benzenesulphonyl chloride in 10.0 mL methanol was added slowly. The reaction mixture was refluxed for 8 h at 70 °C. The completion of the reaction was confirmed by TLC (water-ethanol, 70:30, v/v). The product solution was reduced to one-third of its volume on a rotary evaporator and kept in refrigerator overnight. A white solid (L1) precipitated out and was collected by filtration on Buchner funnel. Finally, the product was washed with cold methanol and hexane followed by drying in a vacuum desiccator over fused calcium chloride. Yield: 83.0%, mol. wt. 331.31 Da, Decomposed over 230 °C, white powder, Anal. Calc. Na₂C₁₁H₁₁SNO₆(%): Calculated C (39.85), H (3.32), N (4.22), S (9.66); Found C (39.82), H (3.39), N (4.28), S (9.77); I.R. (KBr pellets, cm⁻¹): 1178 (νS=O)_{sym}, 908 (νS-N), 1375 (νOCO)_{sym}, 1598 (νOCO) _{asym}, 3488 (νN-H); UV-Vis. (H₂O, nm): 208-219 (n-σ*), 243-272 (π-π*); ¹H NMR (d₆-DMSO): 7.770 (s, SO₂NH, 1H), 7.626 (d, aromatic, 2H), 7.332 (d, aromatic, 3H), 3.592 (t, 1H), 2.082 (m, 2H), 2.310 (t, 2H); ESI-MS: m/z = 663.97 [2M+H⁺]⁺, 372 [M+K⁺+2H⁺]⁺, 352.08 [M+NH₄⁺+3H⁺]⁺, 324.05 [M-Na⁺+NH₄⁺-2H⁺]⁺, 202.97 [M-2(COONa)+H⁺]⁺.

The ligands (L2 and L3) were prepared by a similar procedure using *p*-toluenebenzenesulphonyl chloride and *p*-chlorobenzenesulphonyl chloride, separately and respectively.

L2: Yield: 80%, mol. wt. 345.07 Da, Decomposed over 212 °C, white powder, Anal. Calc. $\text{Na}_2\text{C}_{12}\text{H}_{13}\text{SNO}_6$ (%): Calculated C (41.73), H (3.76), N (4.05), S (13.05); Found C (41.75), H (3.79), N (4.11), S (13.12); I.R. (KBr pellets, cm^{-1}): 1187.0 ($\nu\text{S}=\text{O}$)sym, 900.0 ($\nu\text{S}-\text{N}$), 1414.1 (νOCO)sym, 1582.5 (νOCO)asym, 3381.7 ($\nu\text{N}-\text{H}$); UV-Vis. (H_2O , nm): 215-240 ($n-\sigma^*$), 250-269 ($\pi-\pi^*$); ^1H NMR (d_6 -DMSO): 7.520 (s, SO_2NH , 1H), 7.637 (d, aromatic, 2H), 7.140 (d, aromatic, 2H), 3.667 (t, 1H), 2.06-2.5 (m, 2H), 3.4 (t, 2H), 3.26 (s, CH_3 -, 3H); ESI-MS: m/z = 410.99 $[\text{M}+\text{H}^+]^+$, 360.04 $[\text{M}+3\text{H}^+]^+$, 346.03 $[\text{M}+\text{H}^+]^+$, 338.06 $[\text{M}+\text{H}^+]^+$, 324.05 $[\text{M}+2\text{H}^+]^+$, 320.05 $[\text{M}+\text{H}^+]^+$, 216.99 $[\text{M}+\text{H}^+]^+$.

L3: Yield: 75%, mol. wt. 365.5 Da, m.p. > 270 °C, white powder, Anal. Calc. $\text{Na}_2\text{C}_{11}\text{H}_{10}\text{SNO}_6\text{Cl}$ (%): Calculated C (36.11), H (2.73), N (3.83), S (8.75); Found C (36.19), H (2.67), N (3.89), S (8.65); I.R. (KBr pellets, cm^{-1}): 1188 ($\nu\text{S}=\text{O}$)sym, 903.0 ($\nu\text{S}-\text{N}$), 1330 (νOCO)sym, 1600 (νOCO)asym, 1042 ($\nu\text{Ar}-\text{Cl}$), 3466.5 ($\nu\text{N}-\text{H}$); UV-Vis. (H_2O , nm): 220-235 ($n-\sigma^*$), 245-283 ($\pi-\pi^*$); ^1H NMR (d_6 -DMSO): 7.870 (s, SO_2NH , 1H), 7.723 (d, aromatic, 2H), 7.422 (d, aromatic, 2H), 3.622 (t, 1H), 2.282 (m, 2H), 2.420 (t, 2H); ESI-MS: m/z = 427.95 $[\text{M}+\text{Na}^++\text{K}^+]^+$, 389.95 $[\text{M}+\text{H}^+]^+$, 384.90 $[\text{M}+\text{NH}_4^++\text{H}^+]^+$, 383.90 $[\text{M}+\text{NH}_4^+]^+$, 382.89 $[\text{M}+\text{H}^+]^+$, 362.04 $[\text{M}-3\text{H}^+]^+$, 238.93 $[\text{M}+2\text{H}^+]^+$, 236.9 $[\text{M}+\text{H}^+]^+$.

Synthesis of Complexes (CuL1 to RuL3)

Synthesis of CuL1

A solution of copper chloride dihydrate (0.170 g, 1.0 mM) in 10.0 mL methanol was added drop wise to a stirred solution of L1 (0.594 g, 2.0 mM) in 20.0 mL Millipore water. The mixture was stirred at room temperature for 6 h. The solution of the complex was reduced to one-third of its volume and kept at room temperature for the evaporation of solvent. The solid complex obtained was washed with hexane and methanol, separately and respectively.

Nickel and ruthenium complexes of **L1** as well as copper, nickel and ruthenium complexes of **L2** and **L3** were prepared by a similar procedure. The complexes obtained were kept in vacuum desiccator over fused calcium chloride.

CuL1: Yield: 72.0%, mol. wt. 679.48 Da, Decomposed over 120 °C, light green solid, Anal. Calc. $\text{Na}_2[\text{Cu}(\text{C}_{11}\text{H}_{11}\text{SNO}_6)_2](\%)$: Calculated C (38.84), H (3.22) N (4.12), S (9.4); Found C (38.78), H (3.25), N (4.16), S (9.38); I.R. (KBr pellets, cm^{-1}): 1199.6 ($\nu\text{S}=\text{O}$)sym, 902 ($\nu\text{S}-\text{N}$), 1396 (νOCO)sym, 1621.8 (νOCO)asym, 3497 ($\nu\text{N}-\text{H}$)str, 569.3 ($\nu\text{Cu}-\text{O}$), 488 ($\nu\text{Cu}-\text{N}$); UV-Vis. (H_2O , nm): 205-223 ($n-\sigma^*$), 247-271 ($\pi-\pi^*$), 276-355 (charge transfer band), 788-809 ($^2\text{T}_{2g}\rightarrow^2\text{E}_g$); \wedge_{M} ($1\times 10^{-3}\text{M}$, H_2O): $183\ \Omega^{-1}\text{cm}^2\text{mol}^{-1}$ (1:2 electrolyte); ESI-MS: $m/z = 747.78$ $[\text{M}+3\text{Na}-\text{H}^+]^+$, 387.81 $\{\text{M}-\text{Na}_2[\text{C}_9\text{H}_{11}\text{SNO}_2]-2\text{COO}\}$, 207.82 $\{\text{M}-\text{Na}_2[\text{Cu}(\text{C}_{11}\text{H}_{11}\text{SNO}_6)-2(\text{COO})]+5\text{H}^+\}^+$.

NiL1: Yield: 63.0%, mol. wt. 674.63 Da, Decomposed over 260 °C, light sky blue solid, Anal. Calc. $\text{Na}_2[\text{Ni}(\text{C}_{11}\text{H}_{11}\text{SNO}_6)_2](\%)$: Calculated C (39.12), H (3.26) N (4.14), S (9.48); Found C (39.09), H (3.30), N (4.19), S (9.52); I.R. (KBr pellets, cm^{-1}): 1198.4 ($\nu\text{S}=\text{O}$)sym, 899 ($\nu\text{S}-\text{N}$), 1401 (νOCO)sym, 1623 (νOCO)asym, 3409.1 ($\nu\text{N}-\text{H}$)str, 569.7 ($\nu\text{Ni}-\text{O}$), 486 ($\nu\text{Ni}-\text{N}$); UV-Vis. (H_2O , nm): 210-222 ($n-\sigma^*$), 252-275 ($\pi-\pi^*$), 513-527 ($^3\text{T}_{1g}(\text{F})\rightarrow^3\text{A}_{2g}(\text{F})$), 879-899 ($^3\text{T}_{2g}(\text{F})\rightarrow^3\text{A}_{2g}(\text{F})$); \wedge_{M} ($1\times 10^{-3}\text{M}$, H_2O): $171\ \Omega^{-1}\text{cm}^2\text{mol}^{-1}$ (1:2 electrolyte); ESI-MS: $m/z = 742.93$ $[\text{M}+3\text{Na}-\text{H}^+]^+$, 382.96 $\{\text{M}-\text{Na}_2[\text{C}_9\text{H}_{11}\text{SNO}_2]-2\text{COO}\}$, 202.97 $\{\text{M}-\text{Na}_2[\text{Ni}(\text{C}_{11}\text{H}_{11}\text{SNO}_6)-2(\text{COO})]+5\text{H}^+\}^+$.

RuL1: Yield: 55.0%, mol. wt. 694.01 Da, m.p. > 275 °C, olive drab solid, Anal. Calc. $\text{Na}[\text{Ru}(\text{C}_{11}\text{H}_{11}\text{SNO}_6)_2](\%)$: Calculated C (38.02), H (3.16) N (4.02), S (9.22); Found C (38.07), H (3.22), N (3.98), S (9.17); I.R. (KBr pellets, cm^{-1}): 1199.6 ($\nu\text{S}=\text{O}$)sym, 901 ($\nu\text{S}-\text{N}$), 1386 (νOCO)sym, 1625 (νOCO)asym, 3442 ($\nu\text{N}-\text{H}$)str, 569.3 ($\nu\text{Ru}-\text{O}$), 492 ($\nu\text{Ru}-\text{N}$); UV-Vis. (H_2O , nm): 250-270 ($n-\sigma^*$), 272-282 ($\pi-\pi^*$), 286-335 ($n-\pi^*$), 530-730 ($^6\text{A}_{1g}\rightarrow^4\text{T}_{1g}$); \wedge_{M}

(1×10^{-3} M, H₂O): $131 \Omega^{-1} \text{cm}^2 \text{mol}^{-1}$ (1:1 electrolyte); ESI-MS: 762.01 [M+3Na-H⁺]⁺, 386.05 {M-Na[C₉H₁₁SNO₂]-2COO⁻}, 201.24 {M-Na[Ru(C₁₁H₁₁SNO₆)-2(COO)]+5H⁺}⁺.

CuL2: Yield: 47.0%, mol. wt. 707.54 Da, Decomposed over 160 °C, green amorphous solid, Anal. Calc. Na₂[Cu(C₁₂H₁₃SNO₆)₂](%): Calculated C (40.70), H (3.66) N (3.94), S (9.04); Found C (40.74), H (3.60), N (3.88), S (9.07); I.R. (KBr pellets, cm⁻¹): 1190.2 (νS=O)_{sym}, 905 (νS-N), 1405.5 (νOCO)_{sym}, 1598.2 (νOCO)_{asym}, 3375.5 (νN-H)_{str}, 566.1 (νCu-O), 493 (νCu-N); UV-Vis. (H₂O, nm): 224-245 (n-σ*), 253-275 (π-π*), 284-361 (charge transfer band), 796-812 (²T_{2g}→²E_g); Λ_M (1×10^{-3} M, H₂O): $161 \Omega^{-1} \text{cm}^2 \text{mol}^{-1}$ (1:2 electrolyte); ESI-MS: m/z = 662.95 [M-2Na⁺+H⁺]⁻, 644.82 [M-2Na⁺-CH₃-2H⁺]⁻, 633.99 [M-2Na⁺-2CH₃+2H⁺]⁻, 410.99 [M-2Na⁺-(C₁₀H₁₃SNO₂)-COO⁻+4H⁺]⁺, 360.05 [M-2Na⁺-(C₁₀H₁₃SNO₂)-2COO⁻-2H⁺]⁻, 216.99 {M-2Na⁺-[Cu(C₁₁H₁₆SNO₂)]-4COO⁻+NH₄⁺+3H⁺}⁺.

NiL2: Yield: 55.0%, mol. wt. 702.69 Da, Decomposed over 230 °C, aero blue amorphous solid, Anal. Calc. Na₂[Ni(C₁₂H₁₃SNO₆)₂](%): Calculated C (40.98), H (3.7) N (3.98), S (9.1); Found C (40.93), H 3.67), N (3.95), S (9.14); I.R. (KBr pellets, cm⁻¹): 1189.0 (νS=O)_{sym}, 902 (νS-N), 1416.7 (νOCO)_{sym}, 1620.3 (νOCO)_{asym}, 3418.1 (νN-H)_{str}, 569.7 (νNi-O), 515 (νNi-N); UV-Vis. (H₂O, nm): 225-237 (n-σ*), 239-251 (π-π*), 255-273 (n-π*); 498-509 (³T_{1g}(F)→³A_{2g}(F), 875-896 (³T_{2g}(F)→³A_{2g}(F); Λ_M (1×10^{-3} M, H₂O): $168 \Omega^{-1} \text{cm}^2 \text{mol}^{-1}$ (1:2 electrolyte); ESI-MS: m/z = 662.95 [M-2Na⁺+H⁺]⁻, 355.53 [M-2Na⁺-(C₁₀H₁₃SNO₂)-2COO⁻-2H⁺]⁻, 212.34 {M-2Na⁺-[Ni(C₁₁H₁₆SNO₂)]-4COO⁻+H₂O+3H⁺}⁺.

RuL2: Yield: 63.0%, mol. wt. 722.07 Da, m.p. > 275 °C, black amorphous solid, Anal. Calc. Na[Ru(C₁₂H₁₃SNO₆)₂](%): Calculated C (39.88), H (3.6) N (3.86), S (8.86); Found C (39.85), H (3.63), N (3.81), S (8.89); I.R. (KBr pellets, cm⁻¹): 1186.5 (νS=O)_{sym}, 903 (νS-N), 1417 (νOCO)_{sym}, 1619 (νOCO)_{asym}, 3440 (νN-H)_{str}, 568.3 (νCu-O), 503 (νRu-N); UV-Vis. (H₂O, nm): 225-233 (n-σ*), 253-273 (π-π*), 308-338 (n-π*), 600-890 (⁶A_{1g}→⁴T_{1g}); Λ_M (1×10^{-3} M, H₂O): $129 \Omega^{-1} \text{cm}^2 \text{mol}^{-1}$ (1:1 electrolyte); ESI-MS: m/z = 700.21 [M-Na⁺+H⁺]⁻,

398.92 $[M-Na^+-(C_{10}H_{13}SNO_2)-2COO^- \cdot 2H^+]^+$, 217.14 $\{M-Na^+-[Ru(C_{11}H_{16}SNO_2)]-4COO^-+H_2O+3H^+\}^+$.

CuL3: Yield: 68.0%, mol. wt. 748.48 Da, Decomposed over 130 °C, citron amorphous solid, Anal. Calc. $Na_2[Cu(C_{11}H_{10}SNO_6Cl)_2]$ (%): Calculated C (35.26), H (2.66) N (3.74), S (8.58); Found C (35.31), H (2.71), N (3.69), S (8.55). I.R. (KBr pellets, cm^{-1}) 1176.2 ($\nu S=O$)sym, 911 ($\nu S-N$), 1396.3 (νOCO)sym, 1621.9 (νOCO)asym, 3510 ($\nu N-H$)str, 1044.1 ($\nu Ar-Cl$), 575.9 ($\nu Cu-O$), 492.4 ($\nu Cu-N$): UV-Vis. (H_2O , nm): 219-242 ($n-\sigma^*$), 258-271 ($\pi-\pi^*$), 288-382 (charge transfer band), 798-806 ($^2T_{2g} \rightarrow ^2E_g$); Λ_M ($1 \times 10^{-3}M$, H_2O): $177 \Omega^{-1}cm^2mol^{-1}$ (1:2 electrolyte); ESI-MS: $m/z = 787.51 [M+K^+]^+$, 771.64 $[M+Na^+]^+$, 701.22 $[M-2Na^+]^+$, 668.89 $[M-2Na^+-Cl+2H^+]^+$, 241.32 $\{M-2Na^+-[Cu(C_9H_{10}SNO_2Cl_2)]-3COO^-+H^+\}^+$.

NiL3: Yield: 83.0%, mol. wt. 743.63 Da, Decomposed over 260 °C, bud green amorphous solid, Anal. Calc. $Na_2[Ni(C_{11}H_{10}SNO_6Cl)_2]$ (%): Calculated C (35.5), H (2.68) N (3.76), S (8.60); Found C (35.48), H (2.65), N (3.69), S (8.65); I.R. (KBr pellets, cm^{-1}) 1190 ($\nu S=O$)sym, 916 ($\nu S-N$), 1396.4 (νOCO)sym, 1624.6 (νOCO)asym, 3382.9 ($\nu N-H$)str, 1040.4 ($\nu Ar-Cl$), 568.8 ($\nu Ni-O$), 486.3 ($\nu Ni-N$): UV-Vis. (H_2O , nm): 232-242 ($n-\sigma^*$), 253-279 ($\pi-\pi^*$), 507-519 ($^3T_{1g}(F) \rightarrow ^3A_{2g}(F)$), 862-889 ($^3T_{2g}(F) \rightarrow ^3A_{2g}(F)$); Λ_M ($1 \times 10^{-3}M$, H_2O): $194 \Omega^{-1}cm^2mol^{-1}$ (1:2 electrolyte); ESI-MS: $m/z = 784.74 [M+K^++2H^+]^+$, 782.75 $[M+K^+]^+$, 766.79 $[M+Na^+]^+$, 724.79 $[M-Na^++4H^+]^+$, 722.79 $[M-Na^++2H^+]^+$, 697.66 $[M-2Na^+]^+$, 666.83 $[M-2Na^+-Cl+4H^+]^+$, 664.83 $[M-2Na^+-Cl+2H^+]^+$, 236.93 $\{M-2Na^+-[Ni(C_9H_{10}SNO_2Cl_2)]-3COO^- \cdot 4H^+\}^+$.

RuL3: Yield: 70.0%, mol. wt. 763.01 Da, m.p. > 280 °C, black olive amorphous solid, Anal. Calc. $Na[Ru(C_{11}H_{10}SNO_6Cl)_2]$ (%): Calculated C (34.58), H (2.62) N (3.66), S (8.38); Found C (34.54), H (2.66), N (3.65), S (8.34); I.R. (KBr pellets, cm^{-1}) 1186.4 ($\nu S=O$)sym, 896 ($\nu S-N$), 1355 (νOCO)sym, 1625 (νOCO)asym, 3428.3 ($\nu N-H$)str, 1046 ($\nu Ar-Cl$) 503.6 ($\nu Ru-O$), 495 ($\nu Ru-N$); UV-Vis. (H_2O , nm): 222-238 ($n-\sigma^*$), 250-280 ($\pi-\pi^*$), 280-348 ($n-\pi^*$), 630-865

(${}^6A_{1g} \rightarrow {}^4T_{1g}$); Λ_M ($1 \times 10^{-3} M$, H_2O): $123 \Omega^{-1} cm^2 mol^{-1}$ (1:1 electrolyte); ESI-MS: $m/z = 802.54 [M+K]^+$, $786.32 [M+Na]^+$, $740.21 [M-Na]^+$, $706.23 [M-Na^+-Cl+2H]^+$.

Solution Stability

A qualitative insight into the stability of complexes at physiological pH was obtained by monitoring their UV-Vis. spectra in PBS solution at 7.4 pH, over a period of 24 h. $10^{-4} M$ solutions of the complexes were prepared in PBS at pH 7.4. The hydrolysis and aquation profiles of the complexes were assessed by recording their electronic spectra over 24 h time period at 25 °C.

Molecular Modelling

Molecular modelling was carried out with a semi-empirical PM3 force field as implemented in the hyperchem 8.0 software [36,37]. It is a graphics program with features of structure building, minimum energy geometry optimization and quick molecular display. Polak-Ribiere was chosen as the minimization algorithm with RMS gradient of 0.1 kcal/(Å mol) and 250 energy calculations were carried out.

DNA Binding

UV-Vis. absorption spectrophotometry was used to study the interactions of ligands and their complexes with Ct-DNA at 7.4 pH in double distilled water containing tris-(hydroxymethyl)-amino methane (Tris, $10^{-2} M$). The concentration of the freshly prepared Ct-DNA solution was determined spectrophotometrically at 260 nm ($\epsilon = 6600 M^{-1} cm^{-1}$) [38]. The binding experiments were carried out by adding increasing concentrations of DNA (0.5×10^{-4} to $1.4 \times 10^{-4} M$) to a fixed concentration of ligands and their complexes ($1.6 \times 10^{-4} M$). First of all, λ_{max} and absorbance values of pure DNA, ligands and their metal complexes in buffer solutions were recorded. 2 mL of each solution of DNA and ligand or metal complex were mixed together and their λ_{max} and absorbance values were recorded. The

absorption spectra were recorded after each addition of different concentrations of DNA solution (2.0 mL).

In Silico Studies

Docking studies of the ligands were performed by Intel[®] dual CPU (1.86 GHz) with Windows XP operating system. The 3D structures of the ligands were drawn using Marwin sketch. The so obtained 3D structures were converted to the pdb file format. Ligand preparation was done by assigning Gastegier charges, merging non-polar hydrogens, and saving it in PDBQT file format using AutoDock Tools (ADT) 4.2 [39]. X-ray crystal structure of DNA (PDB ID: 1BNA) was obtained from the Protein Data Bank [40]. Using AutoDock Tools (ADT) 4.2, DNA was saved in PDB file format leaving hetero-atoms (water). Gastegier charges were assigned to DNA and saved in PDBQT file format using ADT. Preparation of parameter files for grid and docking was done using ADT. Docking was performed with AutoDock 4.2 (Scripps Research Institute, USA) considering all the rotatable bonds of ligand as rotatable and receptor as rigid [41]. Grid box size of 60 x 80 x 110 Å^o with 0.375 Å^o spacing was used that included the whole DNA. Docking to macromolecule was performed using an empirical-free energy function and Lamarckian Genetic Algorithm, with an initial population of 150 randomly placed individuals, a maximum number of 2,500,000 energy evaluations, a mutation rate of 0.02, and crossover rate of 0.80. Fifty independent docking runs were performed for each ligand and DNA-ligand adduct for lowest free energy of binding conformation from the largest cluster and saved in PDBQT format. Docking results were analysed using UCSF Chimera [42] for possible polar and hydrophobic interactions.

Cytotoxicity Profiles

Drug significance of the developed compounds was evaluated by investigating their anticancer activities and hemolysis profiles. Hemolysis behaviour of the compounds was

evaluated on rabbit RBCs. In addition, their anticancer profiles were determined on MCF-7 cancer cell lines. Doxorubicin was used as reference drug. Both hemolysis and anticancer assays were carried out in triplicate. These studies were carried out as described below.

Hemolytic Assays

The experimental procedure for evaluating the hemolysis behaviour of the compounds is an adjustment of ASTM standard F-756-00 [43], which is based on colorimetric detection of Drabkin's solution. 1.5 mL of test compounds was incubated in 0.214 mL of dilute blood (0.1 mL rabbit whole blood mixed with 0.9 mL PBS) at 37 °C for 3 h. The hemoglobin in as-harvested plasma of rabbit blood was found to be less than 220 µg/mL (basal level for hemolysis test) to confirm that fresh rabbit blood was used in the test. Following incubation, the solution was centrifuged at 3800 rpm for 15 min. To determine the supernatant hemoglobin, 0.8 mL of Drabkin's solution was added to 0.2 mL of supernatant and the sample was allowed to stand for 15 min. The amount of cyanmethemoglobin in the supernatant was measured by absorbance measurement at 540 nm and then compared to a standard curve (hemoglobin concentrations ranging from 32 to 1068 mg/mL). The percent hemolysis refers to the hemoglobin concentration in the supernatant of a blood sample not treated with test compounds to the obtained percentage of test compound-induced hemolysis. Additionally, the absorption of the test compounds was determined at 540 nm in order to eliminate the effect of absorption of test compounds. Finally, saline solution and double distilled water were used as negative and positive controls, respectively.

Anticancer Assays

The *in vitro* anticancer profiles were determined by testing L1-L3 and CuL1 to RuL3 against human breast cancer cell line; MCF-7, by a cell viability assay (MTT assay) [44]. DMEM (low glucose), 10% fetal bovine serum and antibiotics/antimycotics formed the main constituents of the culture medium. MCF-7 cells were seeded in 96-well plate at a density of

2×10^3 cells/well and were incubated at 37 °C under a humidified atmosphere containing 5% CO₂ for 24 h before assay. After that, the cells were further incubated in media containing various concentrations of the test compounds. After 24 h, the medium was removed and washed with PBS. About, 20 µL of MTT solution was added to each well followed by 4 h of incubation at 37 °C. Subsequently, the medium was removed and 200 µL of DMSO were added. After shaking slowly twice for 5 s, the absorbance of each well was determined at 570 nm. The cell viability (%) was calculated as the ratio of the number of surviving cells in test compound treated samples to that of control.

Results and Discussion

The analytical and spectroscopic data of L1-L3 and CuL1 to RuL3 supported their proposed structures. All the compounds were solids and stable to air. Besides, all the compounds were readily soluble in water, DMSO and DMF. Water solubility of the compounds is an added advantage for their therapeutic applications, since all biochemical reactions are based on small molecules those dissolve in aqueous media [45]. The compounds were purified by washing with cold methanol and hexane.

Glutamic acid was neutralized with aqueous sodium hydroxide to facilitate the condensation of its -NH₂ group with -SO₂Cl group of benzenesulphonyl chlorides. The excess sodium hydroxide neutralized the HCl produced during the condensation of benzenesulphonyl chlorides. The condensation and the subsequent reaction mechanism involved in the formation of ligands is shown in Scheme 1. The ligands (L1-L3) complexed with copper(II), nickel(II) and ruthenium(III) ions to form the complexes (CuL1 to RuL3) as shown in Scheme 2.

The compositions of all the compounds were ascertained on the basis of elemental analysis and ESI-MS spectra. Copper(II) and nickel(II) complexes had molar conductance in the range of 161-183 and 168-194 Ω⁻¹cm²mol⁻¹, respectively, indicating their 1:2 electrolytic

nature. However, ruthenium complexes had molar conductance in the range of 123-131 $\Omega^{-1}\text{cm}^2\text{mol}^{-1}$, which indicated their 1:1 electrolytic nature [46]. It might be inferred from the molar conductance data that the two units of excess negative charge of the copper and nickel complexes were balanced by two sodium ions existing outside their coordination spheres. However, only one sodium ion was needed to balance the one unit of extra negative charge in ruthenium complexes. Finally, it can be assumed from the results of elemental analysis and ESI-MS spectra that 1:2 metal to ligand complexes resulted, wherein metal ions in nickel and ruthenium complexes are in an octahedral environment and those in copper complexes are in a tetragonal environment, which was further supported by their UV-Vis. spectra.

The formation of L1-L3 and CuL1 to RuL3 was confirmed by the appearance of peaks due to S-N stretching vibrations in the range of 896-916 cm^{-1} . Besides, the peaks due to the symmetric and asymmetric vibrations of carboxylate groups were found in the range of 1330-1417 and 1582.5-1625 cm^{-1} , respectively. The monodentate fashioned coordination of the carboxylate groups to the metal ions in the complexes was confirmed by the prominent shifts in both the symmetric and asymmetric vibrations of (-OCO-) groups in the spectra of metal complexes [47-50]. Besides, the stretching frequencies for metal to oxygen and metal to nitrogen (Cu-O, Cu-N, Ni-O, Ni-N, Ru-O and Ru-N) bonds were observed in the spectra of all the complexes; suggesting the coordination of metal ions with the ligand donor atoms. ^1H NMR spectra of the ligands showed the signals of the -NH protons of -SO₂NH group in the range of 7.520-7.870 ppm. Besides, the aromatic protons were observed in the region 7.140-7.723 ppm. The proton signals in the spectra of the complexes were slightly shifted due to the coordinating effect of the metal ions [51,52]. Mass spectra of L1, L2 and L3 showed peaks at m/z values 372.01, 346.03 and 382.89 corresponding to the moieties $[\text{Na}_2\text{C}_{11}\text{H}_{11}\text{SNO}_6+\text{K}^++2\text{H}^+]^+$, $[\text{Na}_2\text{C}_{12}\text{H}_{13}\text{SNO}_6+\text{H}^+]^+$ and $[\text{Na}_2\text{C}_{11}\text{H}_{10}\text{SNO}_6\text{Cl}+\text{NH}_4^+-\text{H}^+]^+$, respectively. Mass spectra of NiL1, CuL2 and NiL3 showed peaks at m/z values 382.96 &

742.93, 644.82 & 662.95 and 766.79 & 782.75 corresponding to $\{\text{Na}_2[\text{Ni}(\text{C}_{11}\text{H}_{11}\text{SNO}_6)_2]-\text{Na}_2[\text{C}_9\text{H}_{11}\text{SNO}_2]-2\text{COO}\}^+$ & $\{\text{Na}_2[\text{Ni}(\text{C}_{11}\text{H}_{11}\text{SNO}_6)_2]+3\text{Na-H}^+\}^+$, $\{\text{Na}_2[\text{Cu}(\text{C}_{12}\text{H}_{13}\text{SNO}_6)_2]-2\text{Na}^+-\text{CH}_3-2\text{H}^+\}^+$ & $\{\text{Na}_2[\text{Cu}(\text{C}_{12}\text{H}_{13}\text{SNO}_6)_2]-2\text{Na}^++\text{H}^+\}^-$ and $\{\text{Na}_2[\text{Ni}(\text{C}_{11}\text{H}_{10}\text{SNO}_6\text{Cl})_2]+2\text{Na}^+\}^+$ & $\{\text{Na}_2[\text{Ni}(\text{C}_{11}\text{H}_{10}\text{SNO}_6\text{Cl})_2]+\text{K}^+\}^+$, respectively. Besides, several fragmentation peaks were observed in the spectra of the compounds in accordance with their proposed structures. UV-Vis. spectra of the ligands showed absorption bands in the regions 208-240 and 243-283 nm corresponding to $n-\pi^*$ and $\pi-\pi^*$ high energy transitions, respectively. The spectra of complexes were characterized by the presence of additional absorption bands due to metal originated d-d transitions characteristic to their geometries. CuL1 to CuL3 showed absorption bands in the ranges from 276-382 and 788-812 nm assigned to charge transfer bands and ${}^2\text{T}_{2g}\leftarrow{}^2\text{E}_g$ transitions, respectively, indicating their tetragonally distorted octahedral geometries [53,54]. NiL1 to NiL3 absorption bands in the ranges from 498-527 and 862-899 nm assigned to ${}^3\text{T}_{1g}(\text{F})\rightarrow{}^3\text{A}_{2g}(\text{F})$ and ${}^3\text{T}_{2g}(\text{F})\rightarrow{}^3\text{A}_{2g}(\text{F})$ transitions, respectively, indicating their octahedral geometries [55-57]. RuL1 to RuL3 showed absorption bands in the ranges from 530-890 nm assigned to ${}^6\text{A}_{1g}\rightarrow{}^4\text{T}_{1g}$ transition, respectively, indicating its octahedral geometry [58-60].

Solution Stability

Aquation is an important step for the proper and safe functioning of many therapeutically active drugs, including the well-known KP1019 and NAMI-A [61,62]. Therefore, the solution stabilities of CuL1 to RuL3 in PBS at physiological pH were assessed by UV-Vis. spectrophotometry. From Fig. 2, it is clear that UV-Vis. spectra recorded; for the fresh solutions of CuL1; showed no intra ligand band shifts after 24 h, however, mild shifts in intensity were observed. In addition, UV-Vis. spectra of NiL1 to RuL3 (Fig. S1) exhibited similar behaviour after 24 h. Moreover, the solutions of the complexes did not precipitate

during this time. All these results indicated the robust nature of the complexes [63-65]. Therefore, the complexes under study did not undergo hydrolysis.

Molecular Modelling

Basically, molecular modeling exploits theoretical methods and computational techniques to mimic the behaviour of molecules. In the absence of crystal structure data of the complexes (CuL1 to RuL3), molecular modelling approach was used to have an insight into their structural information. Energy minimized configurations of complexes are achieved by the applications of molecular mechanics, which therefore, has become a tool of increasing utility for the structural investigation of metal complexes [66,67]. Generally, energy minimization methods are used to obtain the equilibrium configuration of molecules. Molecular systems in their stable states correspond to global and local minima on their potential energy surface. Energy minimization exploits the mathematical procedure of optimization and moves atoms to reduce the net forces (the gradients of potential energy) on the atoms till they are negligible. These studies were carried out by the use of semi-empirical method PM3 as implemented in the hyperchem 8.0 using Polak-Ribiere (conjugate gradient) algorithm keeping RMS gradient of 0.01 kcal/Å mol. The ball and stick models of CuL1 to RuL3 are shown in Fig. 3. The total energies and heats of formation of CuL1 to RuL3 calculated ranged from -747295.87 to -846239.10 and 6.15 to -885.71 kJ/mole, respectively (Table 1). Besides, the surface areas and volumes of the modelled molecules were also calculated and found in the ranges of 279.03-688.89 Å² and 1302.11-1468.76 Å³, respectively for CuL1 to RuL3 (Table 1).

DNA Binding

Majority of the anticancer drugs specifically target DNA and, therefore, DNA binding is one of the most critical steps for the functioning of a large number of metallo anticancer drugs. DNA offers several binding modes (outer-sphere non-covalent binding, metal

coordination to nucleobases and phosphate backbone interactions) to the anticancer drugs [68]. DNA binding is often investigated by electronic absorption spectroscopy by recording the changes in the absorbance and shifts in wavelength [69]. The different spectral absorbances of DNA with complexes are indications of interactions [70,71].

The ratio of the absorbance of the stock solution of Ct-DNA in buffer at 260 and 280 nm was greater than 1.80 ($A_{260}/A_{280} > 1.80$), indicating the protein free nature of DNA [72]. The spectra depicting the interactions of DNA with L1 and CuL1 are given in Figs. 4 and 5, respectively. Besides, the spectra of the interactions of L2, L3 and NiL1 to RuL3 are shown in Figs. S2-S11. Addition of increasing concentrations of DNA solutions; 0.5×10^{-4} , 0.8×10^{-4} , 1.1×10^{-4} and 1.4×10^{-4} M, separately to the ligand and metal complex solutions (1.6×10^{-4} M) resulted in hyperchromic shifts in the range of 17.14-55.55% (Table 1).

These spectral changes indicated that the complexes bound to DNA *via* non-covalent interactions or simply uncoiled DNA double helix and exposed more DNA bases [73]. The non-covalent interactions may include hydrogen bonding between the base pairs (accessible in the minor grooves) with the nitrogen and oxygen atoms of ligands and their complexes. In addition, Van der Waals attractive forces may also be involved in causing the binding of the ligands and complexes. Hyperchromism and hypochromism are indications of the interaction of compounds with DNA helix. Hyperchromic shifts revealed the changes in DNA structure and conformation after the compounds bound to DNA; leading to structural damage of DNA helix [74,75].

For the quantitative determination of DNA binding potentials of L1-L3 and CuL1-RuL3, their binding constants (K_b) were obtained by monitoring the changes in absorbance of the $\pi \rightarrow \pi^*$ spectral band (239-296 nm) with increasing concentrations of DNA by using the following equation [76],

$$[\text{DNA}] / (\varepsilon_a - \varepsilon_f) = [\text{DNA}] / (\varepsilon_b - \varepsilon_f) + 1/K_b(\varepsilon_b - \varepsilon_f)$$

where [DNA] is the concentration of DNA in base pairs, the apparent absorption coefficients ε_a , ε_f and ε_b correspond to $A_{\text{obs}}/[\text{Complex}]$, the extinction coefficient for the free complex and the extinction coefficient for the complex in the fully bound form, respectively. DNA binding constants (K_b) calculated for L1-L3 and CuL1 to RuL3 ranged from 0.7×10^3 - $2.1 \times 10^3 \text{ M}^{-1}$ and 1.8×10^3 - $5.24 \times 10^4 \text{ M}^{-1}$ (Table 1), respectively. These values indicated good binding of ligands and their complexes with DNA. The order of DNA binding of the compounds is $\text{RuL3} > \text{RuL2} > \text{RuL1} > \text{NiL3} > \text{CuL3} > \text{CuL2} > \text{NiL1} > \text{NiL2} > \text{L3} > \text{CuL1} = \text{L2} > \text{L1}$. Metal complexes are generally, known to bind to DNA more strongly as compared to their free ligands due to the presence of additional charge on the central metal ion core and vacant d-orbitals [77]. Ruthenium complexes displayed higher binding constants as compared to copper and nickel complexes due to their uninegative charge [78]. Besides, ruthenium complexes exhibited similar binding constants as seen in the single report on the DNA binding studies of anionic ruthenium complexes [78]. Higher binding constants of CuL2-RuL3 as compared to CuL1 might be attributed to the polarizing and non-polarizing effects of $-\text{CH}_3$ and $-\text{Cl}$ groups in these complexes.

In Silico Studies

Combinatorial chemistry and virtual screening are well reputed possibly due to their reduction of the extremely time-consuming steps of organic and inorganic synthesis and biological screening. Molecular docking is a very useful tool for the prediction of the interactions of drugs with various biological macromolecules at supramolecular level [79]. B-DNA, the most prevalent form of DNA has deep and wide major grooves and deep and narrow minor grooves. It is the base pairing between the two strands of DNA that gives rise to the distinct hydrogen bond acceptor/donor patterns in the major and minor grooves. The rigid molecular DNA docking of the ligands has been carried out using AutoDock 4.2 to find out the possible sites of the interactions of DNA with the ligands. The docking studies of

ligands were performed with DNA dodecamers d(CGCGAATTCGCG)₂ (PDB ID: 1BNA). The molecular docked models of the ligand-DNA adducts of L1, L2 and L3 are shown in Figs. 6, 7 and 8, respectively. It is clear from these figures that the ligands interacted with DNA through minor grooves. Besides, L1, L2 and L3 formed 2, 1 and 6 hydrogen bonds with DNA, respectively. The docking energies of the ligands were in the order as $L2 > L1 > L3$ (Table 2). In addition, the Van der Waals energies of the ligands were in the order as $L2 > L1 > L3$ (Table 2), the same as the order of their docking energy. The greater Van der Waals energy of L2 in comparison to L1 and L3 might be attributed to the presence of methyl group on the aromatic ring of L2. Lower Van der Waals energy of L3 as compared to L1 might be due to the hydrophilicity of chloro substituted aromatic ring. Furthermore, it might be said that the Van der Waals forces have played a more significant role than that played by the number of hydrogen bonds in causing the binding of the ligands to DNA. The maximum number of hydrogen bonds formed by L3 might be attributed to the assistance of the chloro substituted aromatic ring in bringing the hydrogen bond forming portions of L3 in close proximity to the hydrogen bond forming portions of DNA. In case, of L2, the methyl substitution on the aromatic ring might be causing steric hindrance to its hydrogen bonding portions. Overall, the order of the docking energy of the ligands is the same as the order of their DNA binding constants and, therefore, *in silico* studies verified the DNA binding of the ligands.

Hemolysis Assays

During the entry of drugs into animal body, they interact with blood components, particularly RBCs (oxygen carrying blood cells). Therefore, it is quite important to assess the effects of the newly developed drugs on RBCs. *In vitro* hemolysis assay is a widely accepted screening tool for predicting *in vivo* toxicity to host cells [80]. *In vitro* toxicities of the developed compounds were compared with the standard anticancer drug doxorubicin. The

hemolysis results of ligand and its complexes are shown in Fig. 9. A perusal of this figure indicates that L1, CuL1, NiL1, L2, CuL2, NiL2, L3 and CuL3 were the least toxic (5% hemolysis) at 100 $\mu\text{g}/\text{mL}$ concentrations. NiL3 was slightly toxic (6% hemolysis). RuL1, RuL2 and RuL3 were more toxic with 12, 17 and 8% hemolysis at the same concentration. On the other hand, doxorubicin exhibited 42% hemolysis at 100 $\mu\text{g}/\text{mL}$ concentration. Therefore, the reported compounds are quite less toxic towards RBCs in comparison to doxorubicin.

3.6 Anticancer Profiles

Anticancer profiles of L1-L3 and CuL1 to RuL3 were assessed from their percentage viabilities. The effects of the reported compounds on MCF-7 cells were evaluated at 0.0001-1.0 $\mu\text{g}/\text{mL}$ concentration ranges with $10 \times$ dilution factor. The percentage viabilities of the reported compounds are given in Fig. 10. A perusal of the figure indicates that all the compounds were viable in the range of 86-131% at 0.0001 $\mu\text{g}/\text{mL}$ concentration. At higher concentration (0.001 $\mu\text{g}/\text{mL}$), the maximum inhibitions were exhibited by L2 (90% viability) > CuL3 (95% viability) > RuL3 ((97% viability) = CuL1 ((97% viability). Interestingly, at 0.01 $\mu\text{g}/\text{mL}$ concentration, L1 (77% viability) and RuL1 (80% viability) exhibited better anticancer effects than doxorubicin (87% viability). Besides, the maximum antiproliferative effects at 0.1 $\mu\text{g}/\text{mL}$ concentration were exhibited by CuL1 (73% viability) and L1 (86% viability). Moreover, NiL2 (53% viability), L1 (60% viability), CuL1 (68% viability) and CuL2 (68% viability) showed maximum activities among the tested compounds at 1.0 $\mu\text{g}/\text{mL}$ concentration. The anticancer activities of the reported ligands and metal complexes depend on the structure and activity relationship leading to different binding modes with DNA. There was no trend in the anticancer activities of ligands and their metal complexes. However, it was observed metal complexes of the ligands showed higher anticancer activities than ligands. It may be due to the facts that metal complexes have greater affinities for DNA than

ligands. Among all the tested concentrations, the maximum inhibition (53% viability) was observed with NiL2 at 1.0 $\mu\text{g/mL}$.

Conclusion

This paper describes the facile syntheses of copper(II), nickel(II) and ruthenium(III) complexes of a series of disodium sulphonamides of L-glutamic acid. Ligands and their complexes were freely soluble in water, which is one of the most important requirements for a suitable drug. The complexes were robust and resisted hydrolysis in PBS at 7.4 pH. DNA binding constants indicated good binding of the compounds. Complexes bound to DNA more strongly as compared to their ligands. As per *in silico* studies, the ligands preferred to enter into the minor groove of DNA. DNA-ligand adducts were mainly stabilised by hydrogen bonding and Van der Waals attractions. All the compounds were significantly less toxic to RBCs as compared to standard drug doxorubicin. Besides, the compounds showed good anticancer activities on MCF-7 cell lines. In nutshell, the compounds showed encouraging therapeutic properties and, therefore, have good future.

Acknowledgements

The authors are thankful to UGC (University Grants Commission) New Delhi for providing UGC-BSR Meritorious research fellowship to Mr. Waseem A. Wani.

Conflict of Interest

There are no conflicts of interest to declare.

References

1. I. Ali, W. A. Wani and K. Saleem, *Cancer Ther.*, 2011, **8**, 56.
2. I. Ali, Rahis-Uddin, K. Saleem, H. Y. Aboul-Enein and A. Rather, *Cancer Ther.*, 2011, **8**, 6.
3. I. Ali, Rahis-Uddin, K. Saleem, M. A. Rather, W. A. Wani and A. Haque, *Curr. Cancer Drug Targets*, 2011, **11**, 135.
4. I. Ali, W. A. Wani, K. Saleem and A. Haque, *Anticancer Agents Med. Chem.*, 2013, **13**, 296.
5. N. Shah and D. S. Dizon, *Future Oncol.*, 2009, **5**, 33.
6. M. A. Medina, *J. Nutr.*, 2001, **131**, 2539S.
7. I. Ali, W. A. Wani, K. Saleem and A. Haque, *Curr. Drug Ther.*, 2012, **7**, 13.
8. S. Kumar, T. E. Witzig and S. V. Rajkumar, *J. Cell Mol. Med.*, 2002, **6**, 160.
9. I. Ali, W. A. Wani, A. Haque and K. Saleem, *Future Med. Chem.*, 2013, **5**, 961.
10. C. L. Vishwanathan, S. Deb, A. Jain, T. Lokhande and A. Juvekar, *Indian J. Pharm. Sci.*, 2008, **70**, 245.
11. C. Cui, Y. Zhang, L. Wang, H. Liu and G. Cui, *J. Pharm. Pharmacol.*, 2009, **61**, 1353.
12. S. Samanta, S.M. Alam, P. Panda and T. Jha, *Eur. J. Med. Chem.*, 2009, **44**, 70.
13. S. Samanta, K. Srikanth, S. Banerjee, B. Debnath, S. Gayen and T. Jha, *Bioorg. Med. Chem.*, 2004, **12**, 1413.
14. S. Farber, L. K. Diamond, R. D. Mercer, R. F. Sylvester and J. A. Wolf, *The New Eng. J. Med.*, 1948, **238**, 787.
15. Drug information online. Methotrexate side effects. (www.drugs.com/sfx/www.drugs.com/sfx/methotrexate-side-effects.html).

16. Z. Ortiz, B. Shea, M. E. Suarez-Almazor, D. Moher, G. A. Wells and P. Tugwell, *J Rheumatol.*, 1998, **25**, 36.
17. A. Scozzafava, T. Owa, A. Mastrolorenzo and C. T. Supuran, *Curr. Med. Chem.*, 2003, **10**, 925.
18. S. G. Kucukguzel, I. Coskun, S. Aydin, G. Aktay S. Gursoy, O. Cevik, O. B. Ozakpinar, D. Ozsavci, A. Sener, N. Kaushik-Basu, A. Basu and T. T. Talele, *Molecules*, 2013, **18**, 3595.
19. E. E. Gurdal, M. Yarim, I. Durmaz and R. Cetin-Atalay, *Drug Res. (Stuttg.)*, 2013, **63**, 121.
20. M. S. Al-Dosari, M. M. Ghorab, M. S. Al-Said and Y. M. Nissan, *Chem. Pharm. Bull. (Tokyo)*, 2013, **61**, 50.
21. N. Abbassi, H. Chicha, M. Rakib el, A. Hannioui, M. Alaoui, A. Hajjaji, D. Geffken, C. Aiello, R. Gangemi, C. Rosano and M. Viale, *Eur. J. Med. Chem.*, 2012, **57**, 240.
22. S. J. Tan, Y. K. Yan, P. P. F. Lee and K. H. Lim, *Future Med. Chem.*, 2010, **2**, 1591.
23. K. Saleem, W. A. Wani, A. Haque, M. N. Lone, M. F. Hsieh, M. A. Jairajpuri and I. Ali, *Future Med. Chem.*, 2013, **5**, 135.
24. M. Ganeshpandian, R. Loganathan, S. Ramakrishnan, A. Riyasdeen, M. A. Akbarsha and M. Palaniandavar, *Polyhedron*, 2013, **52**, 924.
25. I. Ali, W. A. Wani, K. Saleem and D. Wesselinova, *Med. Chem.*, 2013, **9**, 11.
26. I. Ali, W. A. Wani, K. Saleem and M. F. Hsieh, *Polyhedron*, 2013, **56**, 134.
27. F. Zhang, Q. Y. Lin, X. L. Zheng, L. L. Zhang, Q. Yang and J. Y. Gu, *J. Fluoresc.*, 2012, **22**, 1395.
28. M. Sobiesiak, I. P. Lorenz, P. Mayer, M. Wozniczka, A. Kufelnicki, U. Krajewska, M. Rozalski and E. Budzisz, *Eur. J. Med. Chem.*, 2011, **46**, 5917.

29. A. Buschini, S. Pinelli, C. Pellacani, F. Giordani, M. B. Ferrari, F. Bisceglie, M. Giannetto, G. Pelosi and P. Tarasconi, *J. Inorg. Biochem.*, 2009, **103**, 666.
30. A. Bergamo and G. Sava, *Dalton Trans.*, 2011, **40**, 7817.
31. I. Kostova, *Curr. Med. Chem.*, 2006, **13**, 1085.
32. I. Ali, K. Saleem, D. Wesselinova and A. Haque, *Med. Chem. Res.*, 2013, **22**, 1386.
33. E. M. Nagy, A. Pettenuzzo, G. Boscutti, L. Marchio, L. Dalla Via and D. Fregona, *Chem. Eur. J.*, 2012, **18**, 14464.
34. E. Corral, A. C. G. Hotze, H. Dulk, A. Leczkowska, A. Rodger, M. J. Hannon and J. Reedijk, *J. Biol. Inorg. Chem.*, 2009, **14**, 439.
35. D. Griffith, S. Cecco, E. Zangrando, A. Bergamo, G. Sava and C. J. Marmion, *J. Biol. Inorg. Chem.*, 2008, **13**, 511.
36. P. R. Reddy and N. Raju, *Polyhedron*, 2012, **44**, 1.
37. HyperChem Version 8.0 Hypercube, Inc., USA
38. M. F. Reichmann, S. A. Rice, C. A. Thomas and P. Doty, *J. Am. Chem. Soc.*, 1954, **76**, 3047.
39. M. F. Sanner, *J. Mol. Graphics Modell.*, 1999, **17**, 57.
40. Protein Data Bank. (<http://www.rcsb.org/pdb>).
41. G. M. Morris, D. S. Goodsell, R. S. Halliday, R. Huey, W. E. Hart, R. K. Belew and A. J. Olson, *J. Comput. Chem.*, 1998, **19**, 1639.
42. E. F. Pettersen, T. D. Goddard, C. C. Huang, G. S. Couch, D. M. Greenblatt, E. C. Meng and T.E. Ferrin, *J. Comput. Chem.*, 2004, **25**, 1605.
43. ASTM F756-00, Standard Practice for Assessment of Hemolytic Properties of Materials; ASTM International: West Conshohocken, 2000, PA, USA. DOI: 10.1520/F0756-00.
44. T. Mosmann, *J. Immunol. Methods*, 1983, **65**, 55.

45. T. Nogrady, *Medicinal Chemistry, A Biochemical Approach*, Oxford University press, New York, 1985.
46. I. Ali, W. A. Wani and K. Saleem, *Synth. React. Inorg. Met-Org. nano-Met. Chem.*, 2013, **43**, 1162.
47. T. A. Stephenson, S. M. Morehouse, A. R. Powell, J. P. Heffer and G. Wilkinson, *J. Chem. Soc.*, 1965, 3632.
48. T. A. Stephenson and G. Wilkinson, *J. Inorg. Nucl. Chem.*, 1967, **29**, 2122.
49. K. Nakamoto, *Infrared Spectra of Inorganic and Co-ordination Compounds*, John Wiley & Sons, New York, 1970.
50. H. A. Laila and P. B. Luigi, *Polyhedron*, 1996, **15**, 327.
51. A. Chaudhary and R. V. Singh, *Ind. J. Chem.*, 2004, **43**, 2529.
52. W. Kemp, *Organic spectroscopy*, Macmillan Press Ltd., London, 1975.
53. C. H. Krushna, C. M. Mahapatra and A. K. Dash. *J. Inorg. Nucl. Chem.*, 1977, **39**, 1253.
54. N. N. Greenwood and A. Earnshaw, *Chemistry of the Elements*, Pergamon Press, New York, USA, 1984.
55. R. Atkins, G. Brewer, E. Kokot, G. M. Mocler and E. Sinn. *Inorg. Chem.*, 1985, **24**, 127.
56. B. N. Figgis and J. Lewis, *Modern Coordination Chemistry*, Interscience, New York, USA, 1960.
57. O. M. Adly, *Spectrochim. Acta A Mol. Biomol. Spectrosc.*, 2012, **95**, 483.
58. A. B. P. Lever, *Inorganic Electronic Spectroscopy*, 2nd edn., Elsevier, Amsterdam, The Netherlands, 1984.
59. M. M. T. Khan, D. Srinivas, R. I. Khureshy, N. H. Khan, *Inorg. Chem.*, 1990, **29**, 2320.

60. S. N. Pal and S. Pal, *Eur. J. Inorg. Chem.*, 2003, **2003**, 4244.
61. M. Groessl, C. G. Hartinger, P. J. Dyson and B. K. Keppler, *J. Inorg. Biochem.*, 2008, **102**, 1060.
62. M. Bacac, A. C. G. Hotze, K. vander Schilden, J. G. Haasnoot, S. Pacor, E. Alessio, G. J. Sava and J. Reedijk, *J. Inorg. Biochem.*, 2004, **98**, 402.
63. F. Arjmand, A. Jamsheera and D. K. Mohapatra, *J. Photochem. Photobiol. B*, 2013, **121**, 75.
64. C. Tan, S. Hu, J. Liu and L. Ji, *Eur. J. Med. Chem.*, 2011, **46**, 1555.
65. F. Arjmand, M. Aziz and M. Chauhan, *J. Inclusion Phenom. Macrocyclic Chem.*, 2008, **61**, 265.
66. M. A. El-ghamry, A. A. Saleh, S. M. Khalil and A. A. Mohammed, *Spectrochim. Acta A Mol. Biomol. Spectrosc.*, 2013, **110**, 205.
67. S. Chandra, S. Bargujar, R. Nirwal, K. Qanungo and S. K. Sharma, *Spectrochim. Acta A Mol. Biomol. Spectrosc.*, 2013, **113**, 164.
68. S. Mathur and S. Tabassum, *Biometals*, 2008, **21**, 299.
69. S. Parveen and F. Arjmand, *Spectrochim. Acta A Mol. Biomol. Spectrosc.*, 2012, **85**, 53.
70. Z. D. Xu, H. Liu, S. L. Xiao, M. Yang and X. H. Bu, *J. Inorg. Biochem.*, 2002, **90**, 79.
71. Y. Wang and Z. Y. Yan, *Tran. Metal Chem.*, 2005, **30**, 902.
72. J. Marmur, *J. Mol. Biol.*, 1961, **3**, 208.
73. P. J. Cox, G. Psomas and C. A. Bolos, *Bioorg. Med. Chem.*, 2009, **17**, 6054.
74. J. K. Barton, A. T. Danishefsky and J. M. Goldberg, *J. Am. Chem. Soc.*, 1984, **106**, 2172.
75. C. S. Chow and J. K. Barton, *Meth. Enzymol.*, 1992, **212**, 219.
76. A. Wolfe, G. H. J. Shimer and T. Meehan, *Biochemistry*, 1987, **26**, 6392.

77. M. Chauhan and F. Arjmand, *Chem. Biodivers.*, 2006, **3**, 660.
78. N. Ljubijankic, A. Zahirovic, E. Turkusic and E. Kahrovic, *Croat. Chem. Acta*, 2013, **86**, 215.
79. I. Ali, A. Haque, K. Saleem and M. F. Hsieh, *Bioorg. Med. Chem.*, 2013, **21**, 3808.
80. C. M. Sayes, K. L. Reed and D. B. Warheit, *Toxicol. Sci.*, 2007, **97**, 163.

Captions:

Scheme Captions:

Scheme 1: Mechanistic representation of the formation of ligands (L1, L2 and L3).

Scheme 2: Schematic depiction of the syntheses of ligands (L1-L3) and their complexes (CuL1 to RuL3). Reagents and conditions: **(A)** solid sodium hydroxide, benzenesulphonyl chlorides, reflux at 70 °C for 8 h, **(B)** hydrated metal chlorides.

Figure Captions:

Figure 1: Glutamic acid derivatives with rich history as anticancer agents.

Figure 2: UV-Vis. spectra of CuL1 in PBS at 7.4 pH. The solid red and dashed black lines indicate the spectra of fresh solutions and the spectra of solutions after 24 h.

Figure 3: A perspective view of the ball and stick models of the energy minimized structures of CuL1 to RuL3 created through molecular modelling. Lone pairs have been explicated for clarity. Nitrogen (blue), sulphur (yellow), carbon (cyan), oxygen (red), chlorine (green), copper, nickel and ruthenium (orange). Sodium cations outside the coordination spheres have been ignored for the energy minimization procedures.

Figure 4: Absorption spectra of L1 (1.6×10^{-4} M) in the absence (red dashed line) and presence (solid lines) of increasing DNA concentrations; 0.5×10^{-4} M (blue), 0.8×10^{-4} M (green), 1.1×10^{-4} M (red) and 1.4×10^{-4} M (black). Arrow indicates the hyperchromic shifts on increasing DNA concentrations ($0.5 - 1.4 \times 10^{-4}$).

Figure 5: Absorption spectra of CuL1 (1.6×10^{-4} M) in the absence (red dashed line) and presence (solid lines) of increasing DNA concentrations; 0.5×10^{-4} M (blue), 0.8×10^{-4} M (green), 1.1×10^{-4} M (red) and 1.4×10^{-4} M (black). Arrow indicates the hyperchromic shifts on increasing DNA concentrations ($0.5 - 1.4 \times 10^{-4}$ M).

Figure 6: Docking image showing the ligand (L1) forming two hydrogen bonds with DNA. The Van der Waal's interaction of the ligand with the hydrophobic chains of DNA can also be visualized.

Figure 7: Docking image showing the ligand (L2) forming one hydrogen bond with DNA. The Van der Waal's interaction of the ligand can also be visualized.

Figure 8: Docking image showing the ligand (L3) forming six hydrogen bonds with DNA. The Van der Waal's interaction of the ligand can also be visualized.

Figure 9: Percentage hemolysis potentials of L1-L3 and CuL1 to RuL3 against rabbit RBCs at 100 $\mu\text{g/mL}$ concentrations with respect to doxorubicin (used as standard).

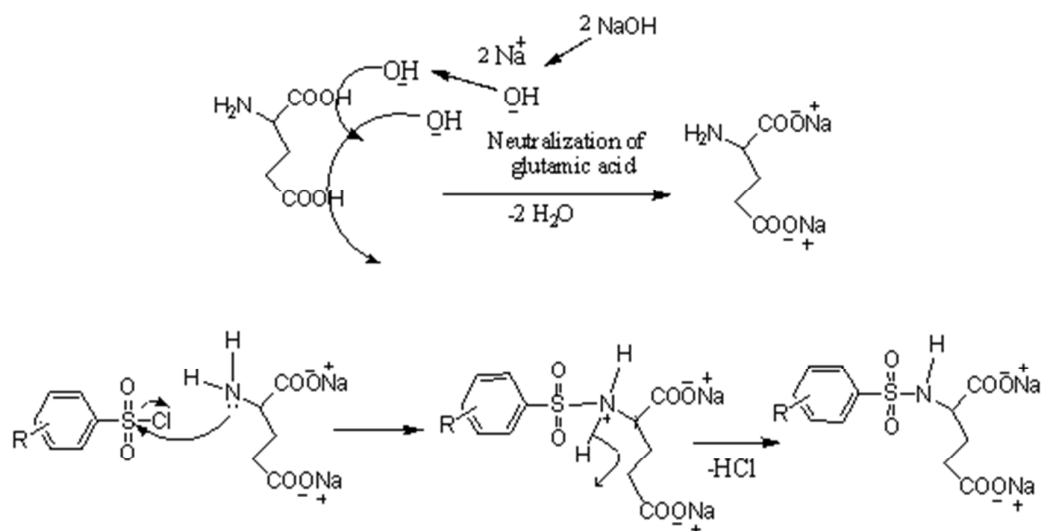
Figure 10: Anticancer activities of L1-L3 and CuL1 to RuL3 with respect to doxorubicin at the concentration range of 0.0001-1.0 $\mu\text{g/mL}$. Anticancer activities have been expressed as percentage viabilities.

Table 1: Percentage hyperchromism, binding constants, heats of formation, surface areas and volumes of the compounds.

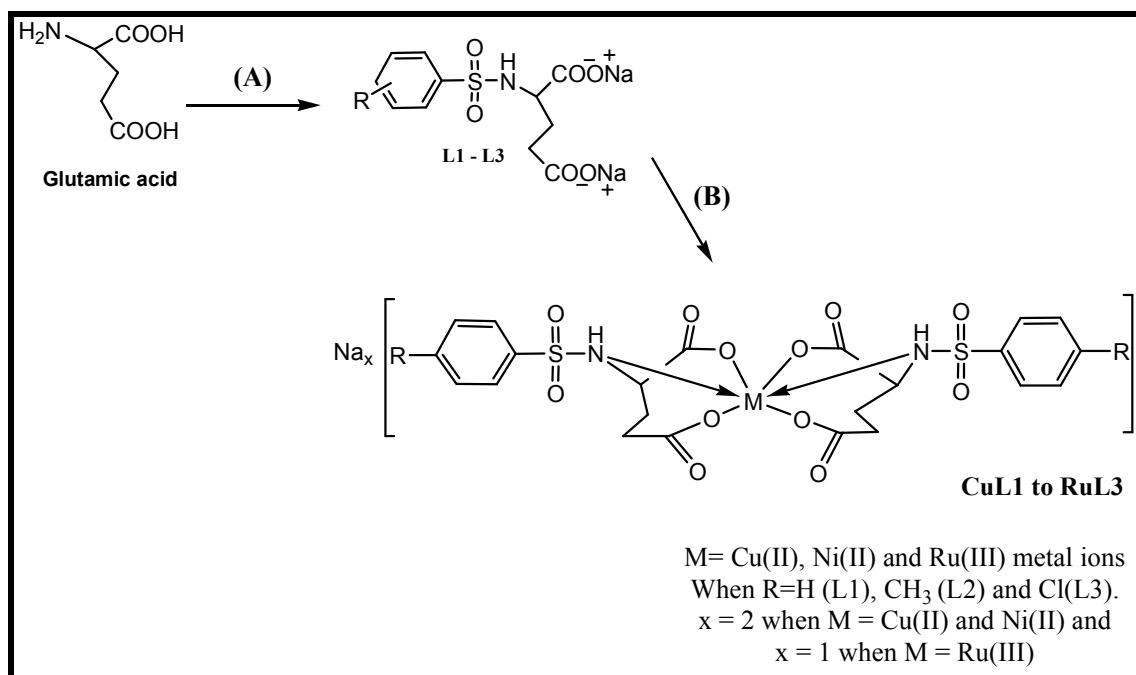
Compounds	% Hyperchromism	K_b (M^{-1})	Total Energy (kJ/mole)	Heat of Formation (kJ/mole)	Surface Area (\AA^2)	Volume (\AA^3)
L1	41.50	0.7×10^3				
CuL1	34.37	1.8×10^3	-800604.21	323.59	469.23	1405.69
NiL1	30.22	3.9×10^3	-787633.81	-885.71	483.82	1468.76
RuL1	41.93	0.97×10^4	-747295.87	539.77	554.18	1328.13
L2	50.01	1.8×10^3				
CuL2	39.65	4.3×10^3	-829733.22	6.15	464.64	1302.11
NiL2	55.55	2.4×10^3	-816114.30	-553.62	489.27	1329.37
RuL2	38.98	1.32×10^4	-776194.76	453.00	619.63	1426.46
L3	17.14	2.1×10^3				
CuL3	27.63	8.1×10^3	-846239.10	244.55	279.03	1374.30
NiL3	44.44	8.5×10^3	-845214.02	-356.35	578.89	1411.12
RuL3	51.11	5.24×10^4	-805411.63	529.15	688.89	1465.17

Table 2: Molecular docking results of L1, L2 and L3.

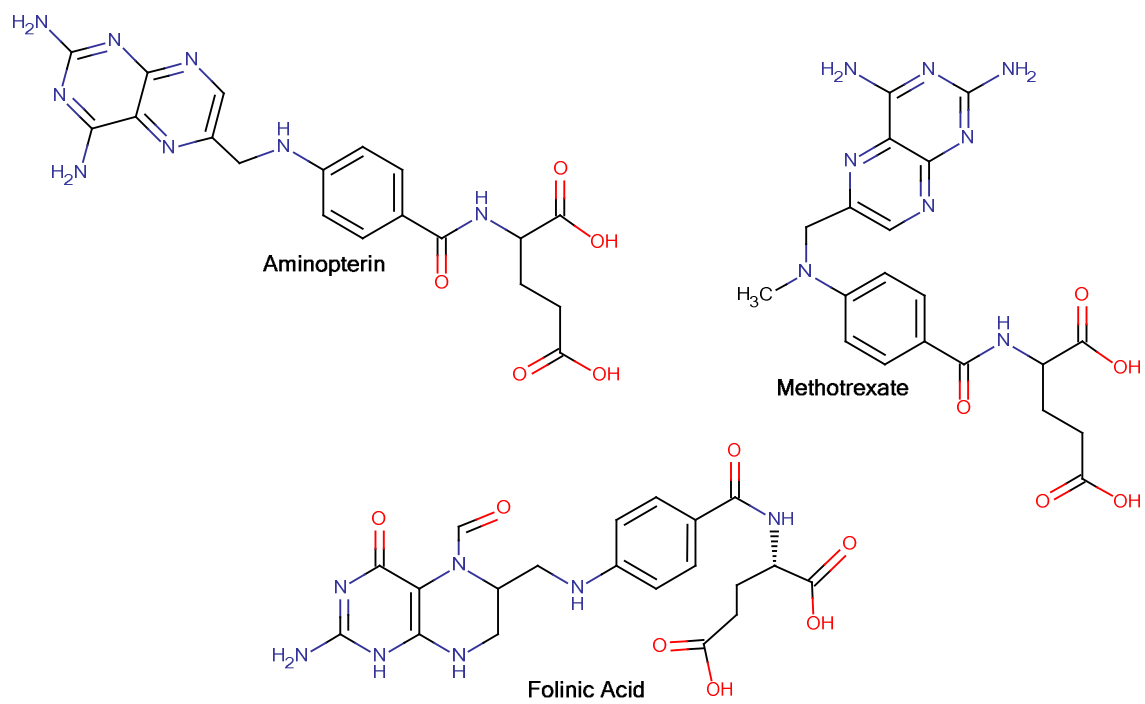
Compounds	No. of hydrogen bounds with DNA	Residues involved in hydrogen bonding	Docking energy (kJ/mole)	Van der Waals energy (kJ/mole)
L1	2	A: DG4:H22 and A: DA5:H3	-12.09	-21.67
L2	1	A:DA5:H3	-15.06	-24.97
L3	6	A: DA6:H7, A: DA6:H6 1, B: DA17:H7, B: DA17 :H6, B: DA18:H7, B: DA 18:H62	-9.70	-19.20



Scheme 1



Scheme 2

**Figure 1**

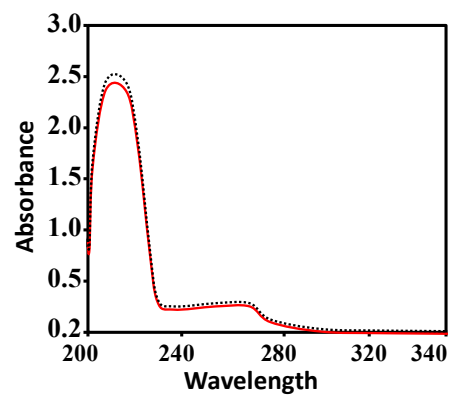


Figure 2

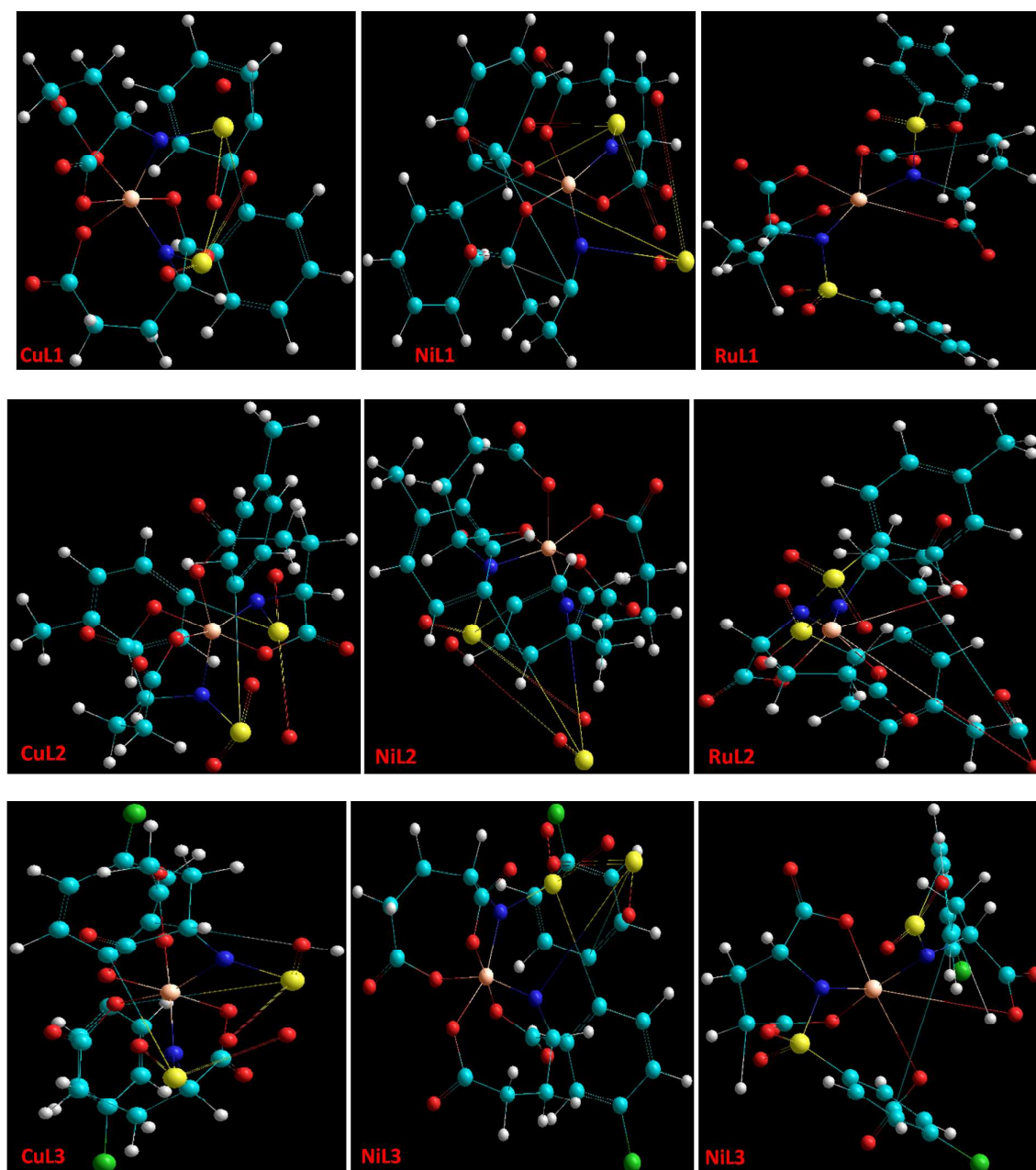


Figure 3

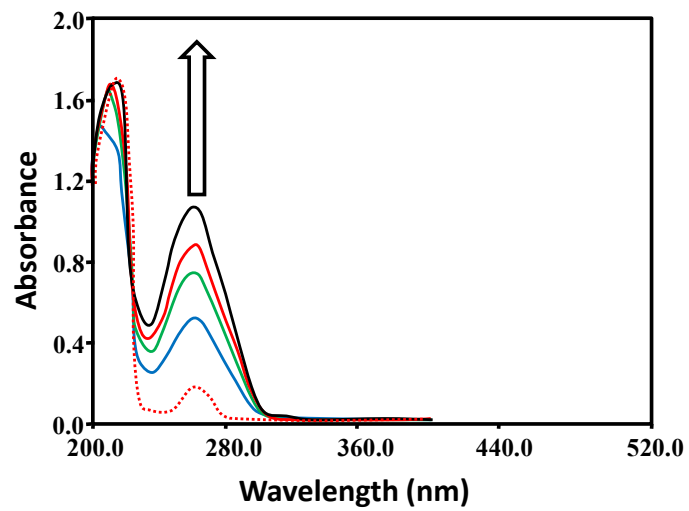


Figure 4

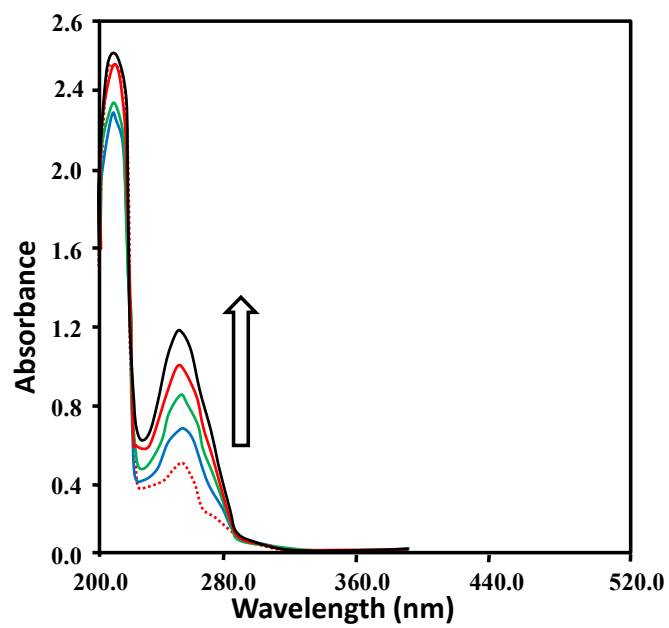


Figure 5

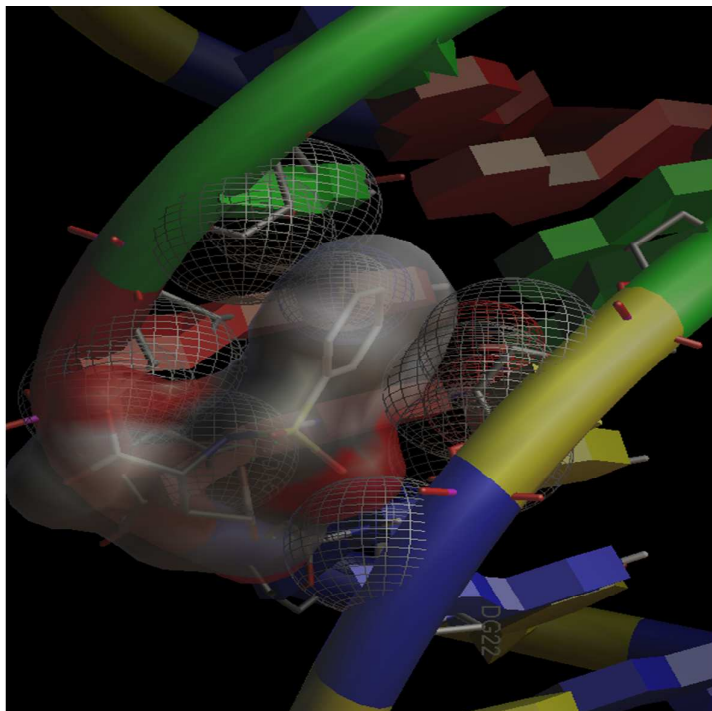


Figure 6

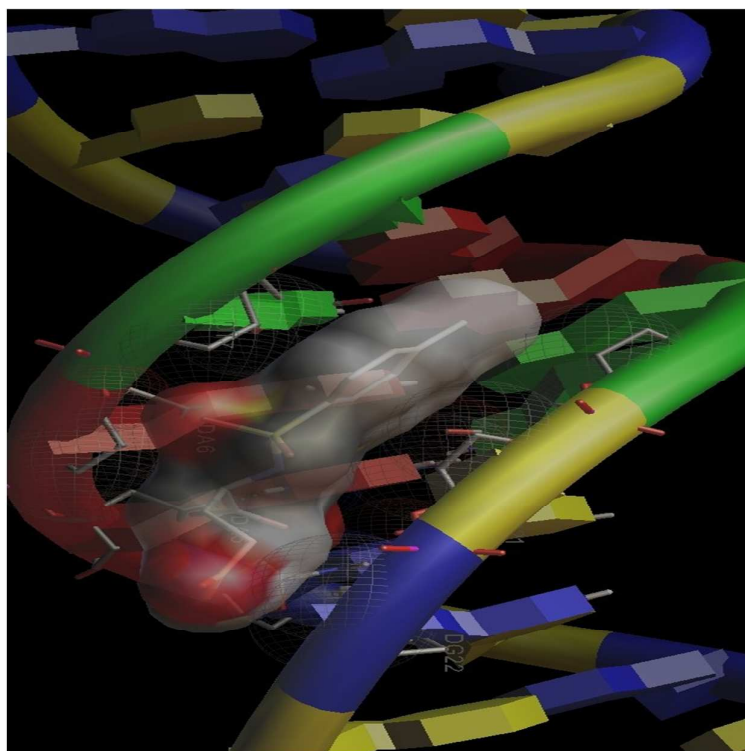


Figure 7

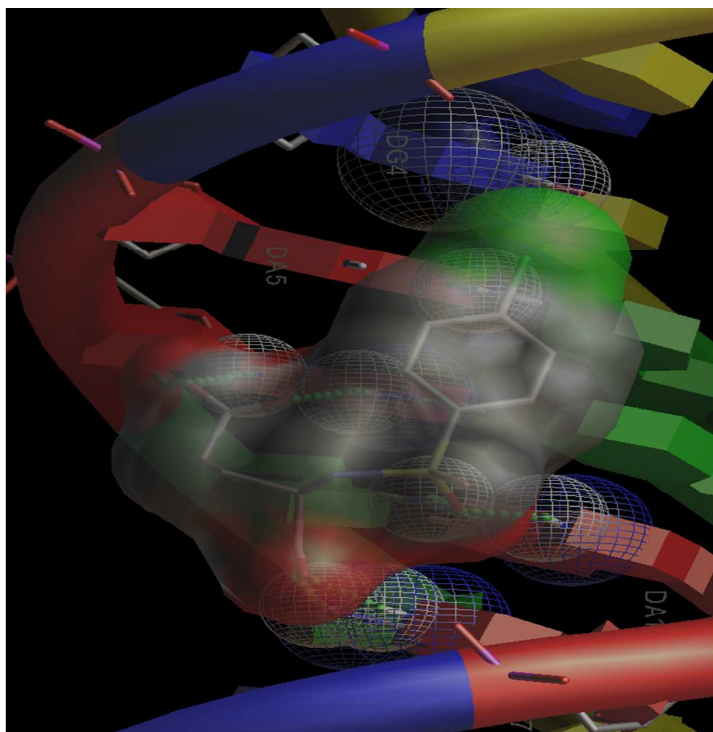


Figure 8

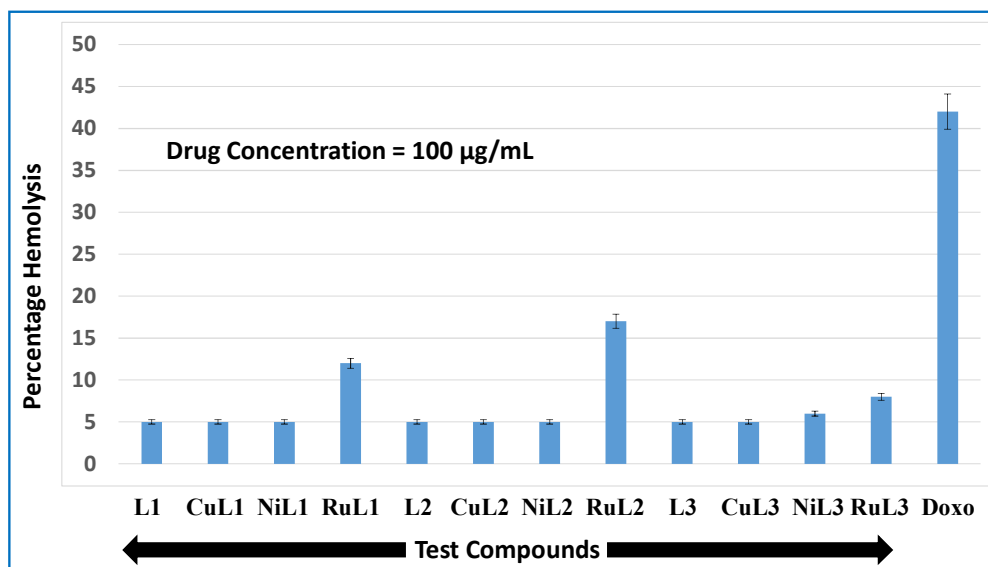


Figure 9

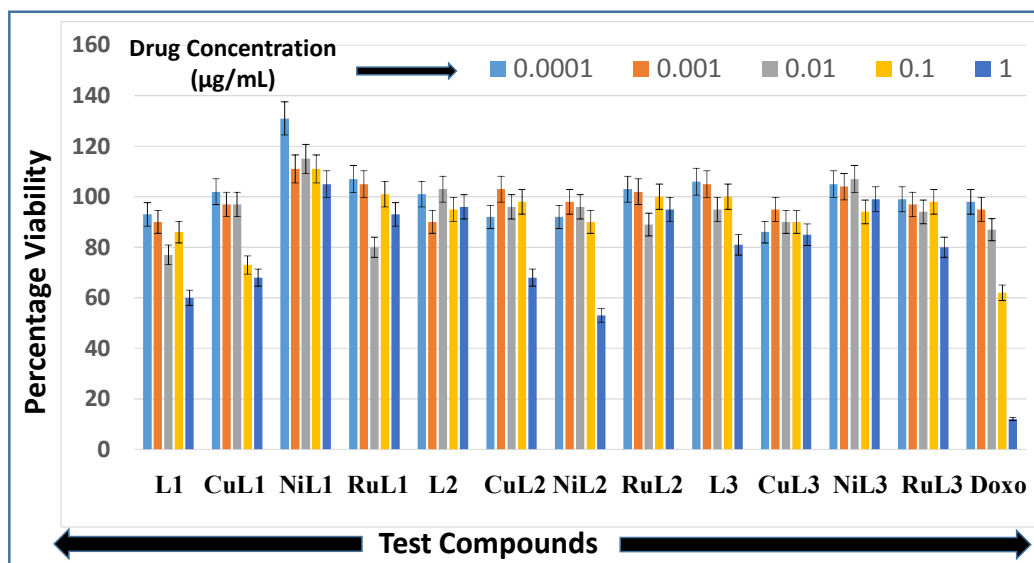


Figure 10